ENVIRONMENTAL EFFECTS ON CYCLIC CRACK EXTENSION

Y. Katz and A. Bussiba*

The experimental program included a study of environmental effects on the steady-state fatigue crack propagation rate and fatigue load/environment interaction effects. AISI 304 austenitic stainless steel, uranium and a uranium alloy were studied, the last two due to their susceptability to ambient environment, which affects the typical fatigue crack propagation curve at low cyclic frequencies. Standard mechanical properties were established and tension-tension fatigue tests were performed. Special attention was given to retardation effects caused by load-environment interaction. The experimental program is described and analysed with emphasis on engineering aspects concerning practical interactive problems.

INTRODUCTION

The role of environmental influences on the fatigue crack extension stage is a many faceted subject. The purpose of the present study however has been to elaborate on certain aspects of this field, in order to deal more effectively with fatigue life prediction and material assessment. Actually, a more complex variation was focused upon, by realizing real fatigue spectra, affected by an aggressive environment. A combined experimental program was followed on two aggressive environments, including studies of steady state fatigue crack propagation rate (FCPR) and fatigue transient effects influenced by environmental factors. In the literature, considerable attention has been directed to elucidating load interaction effects during the fatigue crack growth stage. Most of these studies have been concerned with mechanical and geometrical factors (Mill (1), Knott (2), Matsuoka (3), Katz (4) and Robin (5)).

In contrast, the role of environmental influences imposed during load transients has hardly been explored. Therefore, additional activity along this complex topic appeared necessary.

* Both authors are with the Nuclear Research Center-Negev P.O.B. 9001 Beer-Sheva 84190, ISRAEL.

Increasing the volume of experimental data in various systems might assist in establishing a more general conceptual view on the above mentioned interactive environmental/mechanical effects.

Experimental Procedure

Materials tested included AISI 304 austenitic stainless steel, α-U and U-Ti. The chemical composition for these materials is given in Table 1.

TABLE 1 - Chemical Composition.

Material	Composition wt.%
AISI 304	Cr-18.6, Ni-10, Mn-1.2, Mo-0.22, C-0.05, Si-0.44, S-0.016, P-0.03, Fe-bal.
α - U	Impurities less than 500 ppm.
U - 0.75% Ti	Ti-0.75, impurities less than 150 ppm.

Standard mechanical properties were obtained at ambient temperatures including measurements of the monotonic fracture toughness parameters. Fatigue tests were performed by using rectangular three point bending specimens with geometries as specified in Table 2. The initial machined notch was sharpened and finally was fatigue precracked, at relatively low stress intensity amplitudes.

TABLE 2 - Three Point Bend Specimen - Dimensions.

	Initial Crack Length a_o (mm)	Thickness B (mm)	Width W(mm)	Span S (mm)	Notch geometry
I (AISI 304)	21.5	19	40	100	V-notched with r_{max}=0.25 mm
II(U-Ti)	3	10	10	40	electro discharged pre-crack

Tension-tension cyclic loading was carried out by a closed loop electro-hydraulic machine, utilizing an amplitude controller device. Sinusoidal waveform was applied for low values of R (K_{min}/K_{max}) and the fatigue cumulative damage was activated by controlled ΔK amplitudes. The fatigue crack extension stage covered ΔK values from the near threshold value (ΔKth) up to the critical value ΔK_{fc}. Crack length measurments by electro-potential methods and by direct microscopic observations provided the means of determining the incremental crack extension rates. The stress intensity range was computed according to the following relationship (6).

$$\Delta K = \frac{\Delta P \; S \; Y}{B \; W^{3/2}} \qquad \ldots\ldots\ldots\ldots\ldots\ldots (1)$$

where Y=f(a/w), B and W are the specimens thickness and width respectively.

By controlling the nominal ΔK, the steady-state and the load transient behavior were studied. In the case of load interaction, a single overload was applied at different intensification values. Accordingly, steady-state FCPR behaviour, as well as fatigue retardation curves were obtained with and without environmental influences. Different environments were used for the AISI 304 and the U-systems. For the AISI 304 stainless steel, hydrogen environment was applied, while for the U-systems, the environmental effects were investigated with controlled humidity interaction. For the AISI 304, electrolytic hydrogen charging accompanied the fatigue run by using a built in charging cell. This procedure enabled hydrogenation at the crack front vicinity, simultaneously with the cyclic loading. The hydrogen charging conditions were described by Mathias et al (7), but here the environment was slightly modified in order to reduce hydrogen fugacity. For the sake of completeness, the experimental scheme included an additional selective activity, regarding the environmental effects. Accordingly, uniaxial and compact single edge notched specimens were used in order to extend fundamental information regarding hydrogenation effects in AISI 304 stainless steel (Mathias et al (8)), as well as humidity effects in U-systems; this in terms of susceptability and related micro-craking events.

In addition, acoustic emission (AE) tracking was performed as complementary information, in parallel to the mechanical and the fractographical studies. SEM fractography was carried out which centered on fracture mode classification, mode transition and micro-cracking occurrence. Actually, the program was oriented towards a comparative study which included, hydrogen-free testing of the AISI 304 stainless steel, and inert gas experimentation in the U-systems. This of course in addition to fatigue with aggressive environment, resulting in load/environment interaction during the fatigue process.

Experimental Results.

The mechanical properties at 296K are summarized in Table 3.

TABLE 3 - Mechanical Properties of the Selected Materials.

Material	Yield Stress $\sigma_{0.2}$ (MPa)	Ultimate Tensile Stress σ_{UTS} (MPa)	Elongation e (%)	Hardness	Critical Stress Intensity Factor Kc (MPa·$m^{1/2}$)
AISI 304*	416	660	45	$90R_b$	82
α-U **	500	840	22.5	$86R_b$	33
U-Ti ***	940	1500	17.5	$45R_c$	50

* as received.
** double rolled and recrystallized material.
*** quenched and aged material.

For background data the role of the interactive effects due to the aggressive environment in monotonic and dynamic conditions, are now illustrated and described. In Figs. 1 and 2 the steady state FCPR curves are shown for the AISI 304 stainless steel and the U-Ti alloy respectively. More data regarding the environmental effects in steady state fatigue are given in Table 4.

Fig. 3 illustrates delayed retardation curves after a single overload for hydrogen free and hydrogenated AISI 304 stainless steel specimens. The tests were performed for a q value of 2 and at a fatigue amplitude of 22MPa·$m^{1/2}$ before and after the applied overload.

In Fig. 4 typical humidity influences in α-U are shown, as obtained from SEN specimens tests. Similarly, the total elongation dependency on $\dot{\varepsilon}$ is demonstrated in Fig. 5 for uniform tensile specimens, emphasizing the significant role of the time dependent component. During this particular static test (controlled by specific plastic off-set values) micro-cracking initiated and propagated in the α-U as shown in Fig. 6. In Fig. 7 the corresponding AE activity in the uniaxial tensile and the SEN specimens are presented. Figs. 8 and 9 illustrate the typical retardation curves as obtained in the U-Ti alloy during the subsequential fatigue run after a single overload. Two base line values are shown which correspond to cyclic amplitudes of 16.5 and 24 MPa·$m^{1/2}$ and for q values of 1.8 and 2.6. The humidity effects are readily noticed, as compared to the FCPR

TABLE 4 - Selected values of Steady-State FCPR at Various ΔK, Environments and Frequencies.

Material		U-0.75% Ti		AISI 304		
	f	Stress Intensity Factor Range				
	Hz	$MPa \cdot m^{\frac{1}{2}}$				
Environment		16.5	24	22	33	44
RH = 40%	1		$5x10^{-4}$			
	30		$2x10^{-4}$			
RH = 80%	1	$7.8x10^{-5}$	$6x10^{-4}$			
	30	$4x10^{-5}$	$1.8x10^{-4}$			
Argon	30	$2.5x10^{-5}$	$9.5x10^{-5}$			
Hydrogen Free	10			$5.2x10^{-5}$	$1.5x10^{-4}$	$3.2x10^{-4}$
Cathoding Charging	1			$1.4x10^{-4}$	$6x10^{-4}$	$1x10^{-3}$
	10			$9x10^{-5}$	$2.5x10^{-4}$	$9x10^{-4}$
	80			$5.6x10^{-5}$	$1.8x10^{-4}$	$5x10^{-4}$

results in argon.

The mode transition in the AISI 304 stainless steel caused by hydrogen charging, is shown in Fig.10. In hydrogen free material, ductile striations are clearly observed (Fig.10(a)) which differ completely from the low energy typical mode in the hydrogenated specimens (Fig.10(b)). This alternative fatigue fracture mode includes also a significant crystallographic habit which is a well known cracking mode in the case of hydrogen damage in stainless steel.

The overload crack front is shown in Fig.11(a) with a clear distinction between the steady-state fatigue striations and the restricted stretched zone activated by the applied overload. Fig.11 (b) shows the ill-defined zone with some abrasive features. Fig.12 illustrate the fatigue crack tip branching after the overload in the U-Ti system tested in 80% humidity and 1Hz. Fig.13 illustrates the environmental and frequency effects as reflected from the typical fractographic findings. High humidity or low frequency values caused secondary cracking and crack branching, which were focussed locally and partially rejoined the major fatigue crack.

The enhaced FCPR for $\Delta K=22$ MPa·$m^{1/2}$ in high humidity is observed microscopically by the increase in striation separation which is consistent with the macroscopical crack extension rate results.

Discussion.

The environmental effects actually caused significant enhancement of the steady state fatigue crack propagation rate values as determined for the AISI 304 stainless steel and for the α-U and the U-Ti alloy. However, it seems advisable to examine the fatigue transient behavior due to the single overload, by considering some of the tendencies as reflected from the current experimental study. Firstly, it appears that the tendencies of the AISI 304 stainless steel and the U-system are quite similar. This applies to the retardation curve profile including the observed shifting of the curves to lower values of $(a-a_o)_{min}$ [the incremental distance which correspondes to $(da/dN)_{min}$] caused by the environmental interaction. This behaviour confirms the results of Ranganathan and Petit (9), which have been obtained from the investigation of 2024 T351 Al-alloy in air and vacuum.

In fact the dependency of fatigue processes on the effective stress intensity range (ΔK_{eff}) is well reflected in the environment tests as witnessed by a phenomenological resemblance of the typical retardation curves. Quantitatively , significant differences occur due to the environment, namely, higher FCPR values developed which caused a significant reduction in the total transient "life".

Some complications arise in the U-0.75Ti alloy in the case of 80% humidity where the damage is not confined to a single advancing fatigue crack. The problem of branching is introduced with effects on the ΔK_{eff}. Moreover, the exceptional behavior of the parameter $(a-a_o)_{min}$ is attributed to the increase of the ill defined zone due to the single overload. Excluding the range where crack growth by the environment is slightly affected by the nominal ΔK (for example in stress corrosion crack extension-stage II), the known description of the retardation curves are preserved even in an aggressive environment. This is expected from the constitutive relationship of both factors namely, fatigue and environmental damage effects. Crack branching affect ΔK_{eff} in addition to the localized crack tip residual stresses activated by the applied overload. In the range of combined effects on ΔK_{eff} certain variations of the typical delayed retardation curve profile are expected as actually observed experimentally (Fig. 9).

It seems that more experimental activity should be invested in the current problem mainly in extending the work to other environment/metal systems. This is particularly important with respect to engineering concepts and data, related to real spectra analysis and life prediction. At this stage, the authors believe it appropriate

to express the environment interactive problem in a more mechanical oriented procedure. This might simplify the problem which involves possible influences of the fatigue driving force factor, as well as the material resistance to cyclic loading. For example, one possibility will be to adopt the approach of a modified intensification value q* appropriate for a specific aggressive environment. This approach is being now examined, and proposed modifications to existing retardation models will be addressed separately.

The AE tracing and the fractographic findings clarify the sequential events which take part in the present fatigue interactive study . Generally, the effective stress intensity range is reduced in the transient zone which was formed by the single overload . In this zone, ΔK_{eff} is below the base-line range value with geometrical (the affected plastic zone size) and environmental effects on the transient "life". The observed fatigue mode transition due to the aggressive environment modify and reduce the load interaction influences, and even affect the early stages of the overload stretched zone. Comparison between the present behaviour (Fig.11(a) with that of the underaged Al-7075, which has been addressed by Katz et al (10), really emphasizes the fine scale differences between the two metallic systems.

In conclusion, the selected metal/environment systems, clearly show the sensitivity of the fatigue crack extension rate to load interaction, even in an aggressive environment. Typical retardation curves due to a single overload are qualitatively preserved. Clearly, additional aspects are introduced by the environmental influences concerning the transient life. The U-systems are quite useful in studing environmental effects on cyclic crack extension, including the complex aspects of fatigue load interaction influences in aggressive environments.

Acknowledgments

The authors wish to thank Mr. M. Kupice of the Nuclear Research Center-Negev for experimental assistance during the present investigation.

SYMBOLS USED

a_o	- initial crack length (mm)
$(a-a_o)_{min}$	- incremental crack extension corresponding to the minimum FCPR value (mm)
AE	- acoustic emission
B	- specimen thickness (mm)
da/dN	- fatigue crack growth rate (mm/cycle)
$(da/dN)_{min}$	- minimum fatigue crack growth rate (mm/cycle)
da/dt	- environmental crack growth rate (mm/sec)
e	- elongation (%)

FCPR -fatigue crack propagation rate

f =frequency (Hz)

K_c =critical stress intensity factor ($MPa \cdot m^{1/2}$)

K_{min} =minimum stress intensity factor ($MPa \cdot m^{1/2}$)

K_{max} =maximum stress intensity factor ($MPa \cdot m^{1/2}$)

q =the peak/base line stress intensity ratio ($\Delta K_{ol}/\Delta K$)

q^* =peak/baseline ratio under environmental conditions

R =stress intensity factor ratio (K_{min}/K_{max})

RH =relative humidity (%)

ΔK =cyclic stress intensity factor range ($K_{max}-K_{min}$) ($MPa \cdot m^{1/2}$)

ΔK_{eff} =effective stress intensity factor range ($MPa \cdot m^{1/2}$)

ΔK_{fc} =fatigue critical stress intensity factor ($MPa \cdot m^{1/2}$)

ΔK_{th} =threshold stress intensity factor range ($MPa \cdot m^{1/2}$)

ΔP =load range (KN)

$\dot{\varepsilon}$ =true strain rate (sec^{-1})

REFERENCES

(1) Mill, W.J. and Hertzberg, R.W., Eng. Fract. Mech. vol.7., 1975, pp.705-711.

(2) Knott, J.F. and Pickard, A. C., Met. Sci. vol.13., 1977 pp.399-404.

(3) Matsuoka, S. and Tanaka, K., J. Mat. Sci. vol.13., 1978 pp.1355-1353.

(4) Katz, Y., Bussiba, A. and Mathias, H., Experimentation and Design in Fatigue, Edited by F.Sherrate and J. B. Sturgeon Wesbury House, IPC Science and Technology Press , Guilford Surrey, U.K. 1981, pp. 147-158.

(5) Robin, C., Chehimi, C., Louah, M. and Pluvinage G., Fracture and the role of microstructure;4th European Con. on Fracture Edited by K. L. Maurer, EMAS, U.K., 1982, pp. 488-495.

(6) ASTM Standarts vol.10., Philadelphia, U.S.A.,1977, pp.505-524

(7) Mathias, H., Katz, Y. and Nadiv , S., Met. Sci. vol.12, 1978, pp.129-137.

(8) Mathias, H., Katz, and Nadiv , S., Metal-Hydrogen System, Edited by T.N.Veziroglu Pergamon Press, 1982, pp.225-249.

(9) Rangnathan, N. and Petite, J., Fatigue Mechanism:Advances in Quantitative Measurement of Physical Damage, ASTM STP 811, Edited by J. Lankford, D. L. Davidson, W. L. Morris and R.P. Wei, ASTM,Philadelphia, Pa., U.S.A., 1983, pp.464-484.

(10) Katz, Y., Bussiba, A. and Mathias, H., Met. Sci., vol.15 1981, pp.317-319.

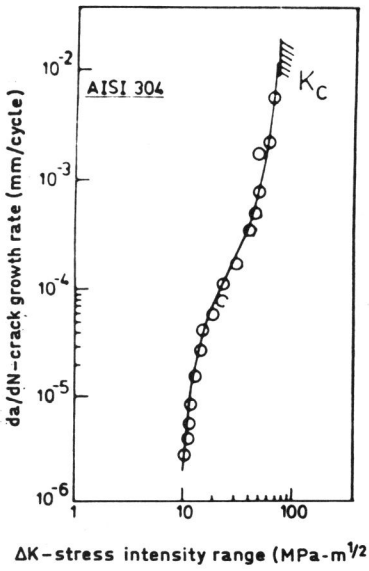

Figure 1 FCPR vs. ΔK in AISI 304 stainless steel.

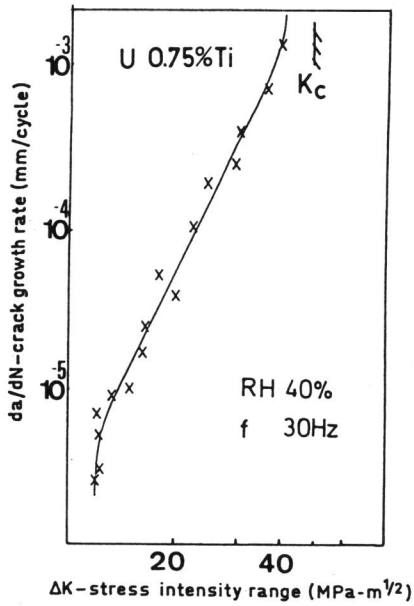

Figure 2 FCPR vs. ΔK in U-Ti alloy.

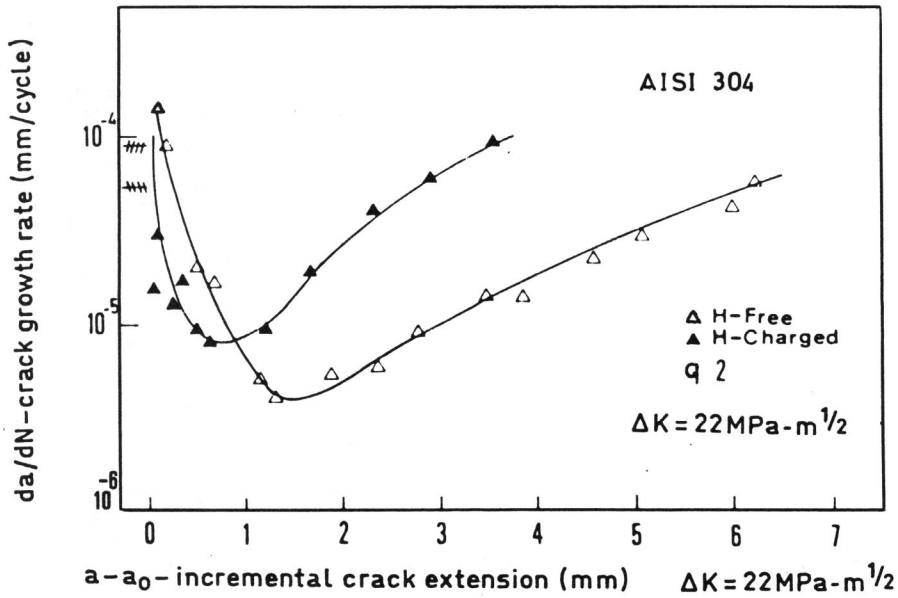

Figure 3 Retardation curves in AISI 304 stainless steel for H-free and H-charged specimens.

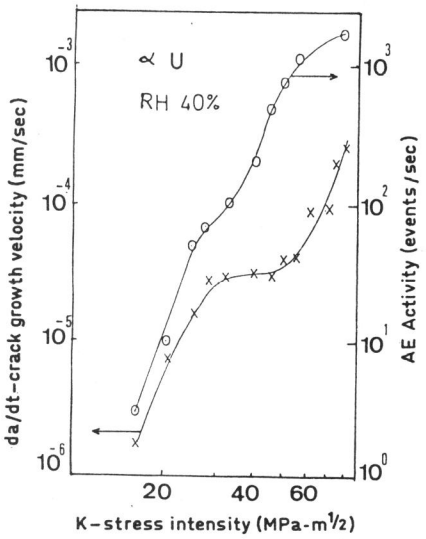

Figure 4 Environmental crack extension and AE in α-U.

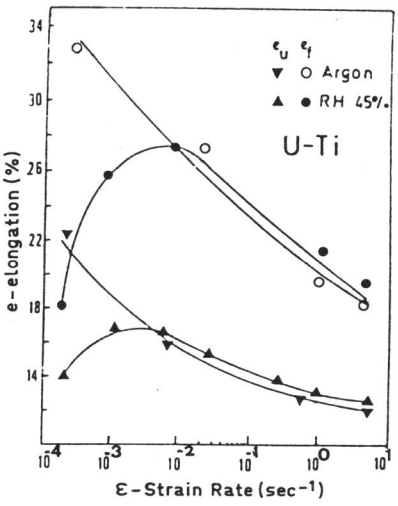

Figure 5 Elongation vs. $\dot{\varepsilon}$ in U-Ti alloy.

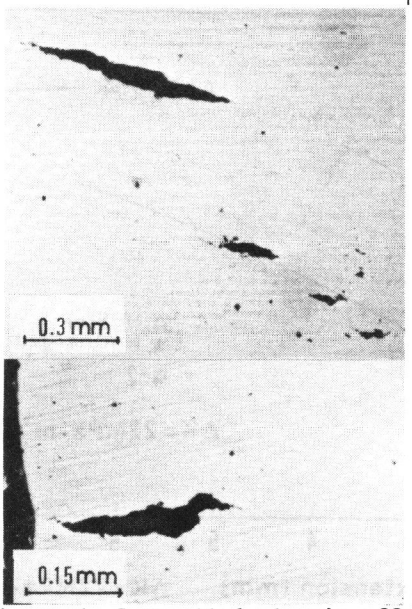

Figure 6 Controlled plastic off-set test- Micro-cracking in α-U.

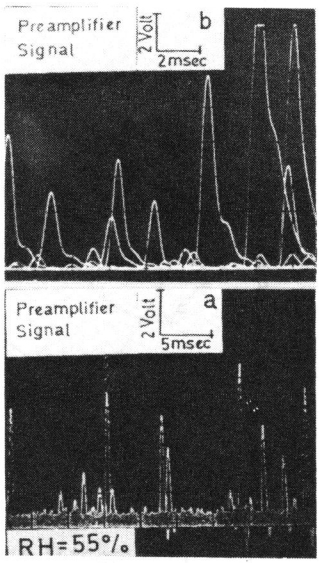

Figure 7 AE activity in α-U for(a) Uniform specimen (b) SEN specimen.

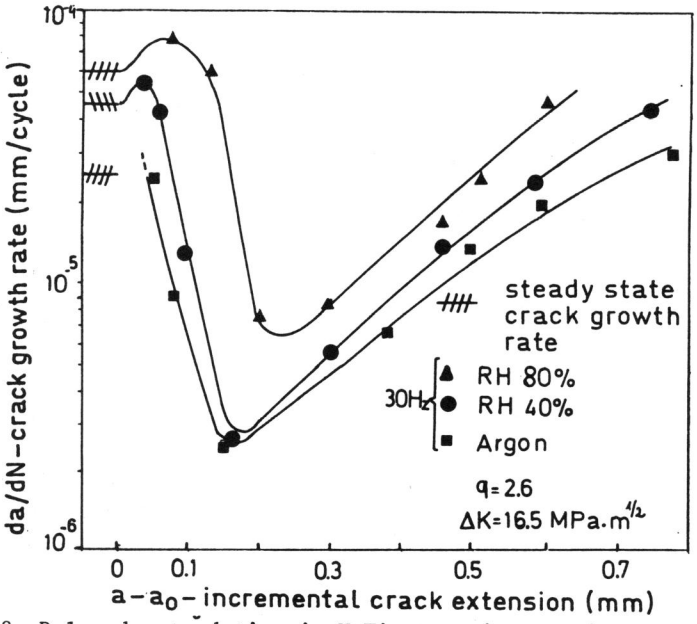

Figure 8 Delayed retardation in U-Ti at various environments-base-line $\Delta K=16.5$ MPa$\cdot m^{1/2}$

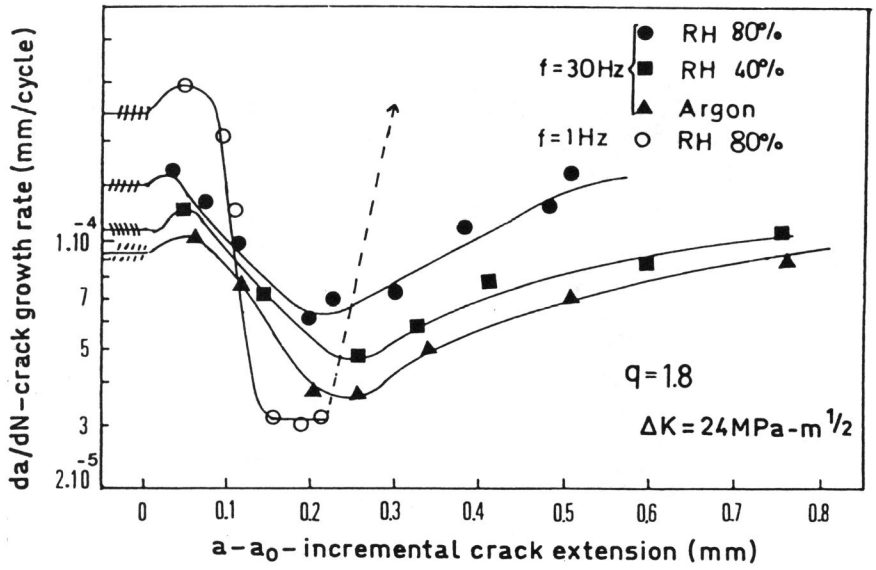

Figure 9 Delayed retardation in U-Ti at various environments-base-line $\Delta K=24$ MPa$\cdot m^{1/2}$

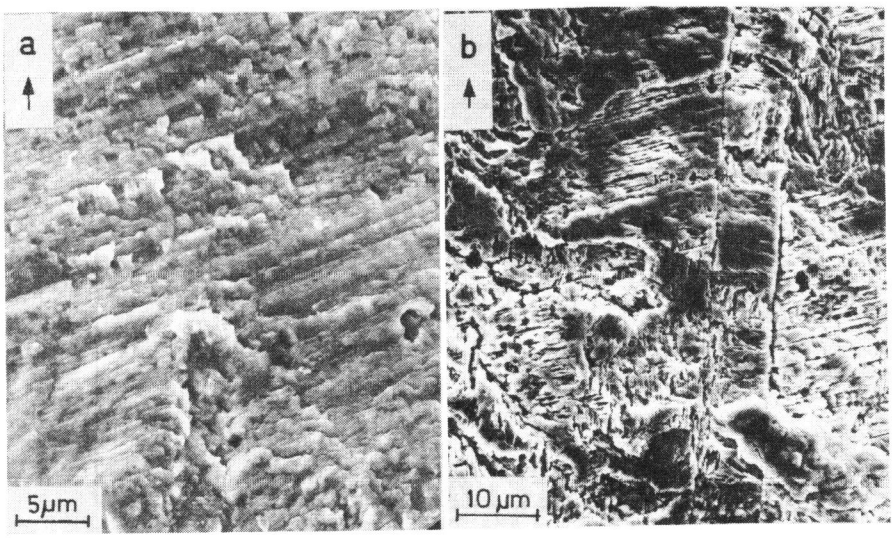

Figure 10 SEM fractography in AISI 304 (a) H-free at $\Delta K=22$ MPa·m$^{1/2}$ (b) after H-charged at $\Delta K=24$ MPa·m$^{1/2}$

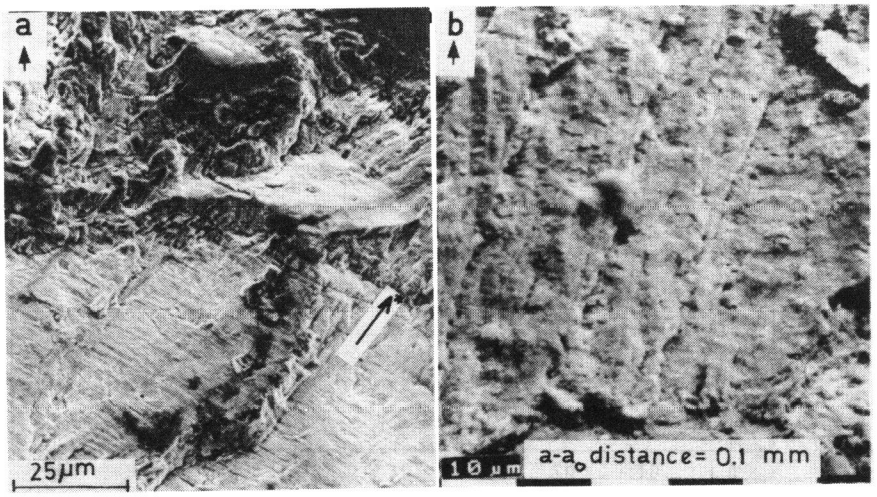

Figure 11 SEM fractography in U-Ti (a) the overload appearance (b) ill defined zone q=1.6, $\Delta K=22$ MPa·m$^{1/2}$. →*-overload crack front.

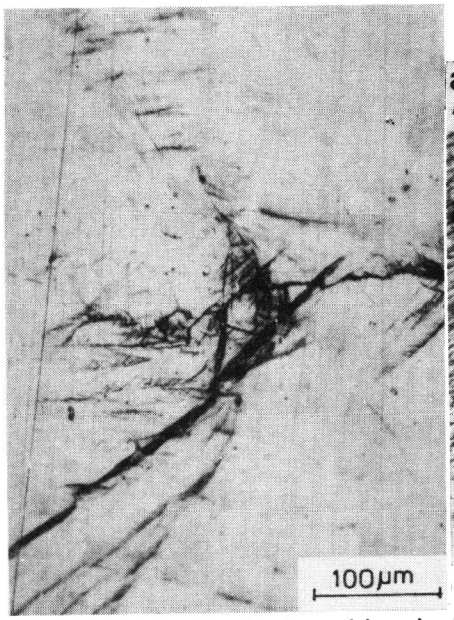

Figure 12 Crack tip branching in fatigue after overload in U-Ti.

Figure 13(a) Typical striations in U-Ti at RH=30% and f=30Hz.

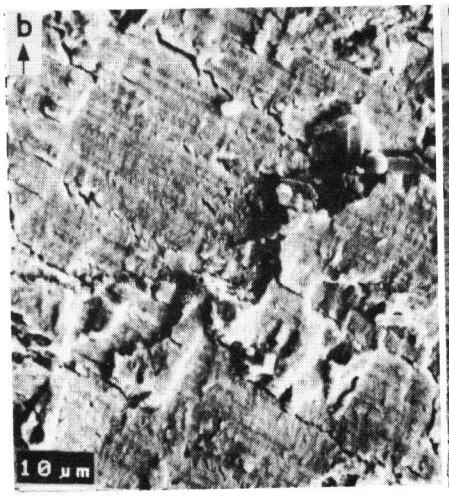

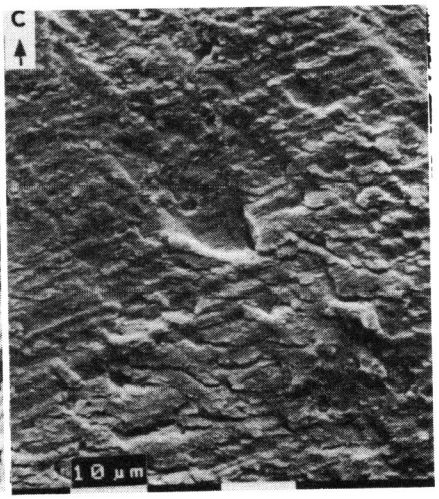

Figure 13(b),(c) Secondary cracking, branching in fatigue at RH-80% f=80Hz (b), f=1Hz(c). ΔK=22 MPa·$m^{1/2}$